Optik - International Journal for Light and Electron Optics 219 (2020) 165204

Contents lists available at ScienceDirect

Optik

journal homepage: www.elsevier.com/locate/ijleo

Original research article

Structural, electrochemical and optical properties of Ni doped ZnO: Experimental and theoretical investigation

Zhanhong Ma[a,b], Fengzhang Ren[a,*], Yafeng Deng[a], Alex A. Volinsky[c]

[a] School of Materials Science and Engineering, Henan University of Science and Technology, China
[b] Henan Collaborative Innovation Centre of Non-Ferrous Generic Technology, Luoyang 471023, China
[c] Department of Mechanical Engineering, University of South Florida, Tampa, FL 33620, USA

ARTICLE INFO

Keywords:
Ni doped ZnO
Absorption spectrum
Electrochemical properties
First principle calculations

ABSTRACT

Pure and Ni-doped ZnO nanorod array films were prepared by the hydrothermal method. The effects of Ni doping on the phase composition, microstructure, and optical and electro-chemical properties of ZnO were investigated. The main crystalline phase of the powders before and after Ni doping is wurtzite ZnO. The luminescent peaks are significantly reduced after Ni doping. The light transmission and is the strongest when the doping concentration is 2 %. The light absorption spectrum confirms that the band gap decreased first and then decreased with the increase of Ni^{2+} doping concentration. According to the M–S (Mott - Schottky) plots, the Ni-doped ZnO is an n-type semiconductor. The current density initially increases with the increased Ni doping amount, and then decreases. First-principles calculation results of nickel-doped zinc oxide show that the energy level of impurities is formed after nickel ions replace zinc ions, which causes the conduction band is shifted down and the band gap is reduced. The impurity energy level causes a slight upward shift in the valence band, which increases the band gap. The calculated results are consistent with the experimental results.

1. Introduction

ZnO semiconductor materials are widely used in new solar cells, photocatalytic degradation, gas sensors and other fields due to their good photoelectric conversion, photocatalysis, gas sensitivity, stable chemical properties and non-toxicity [1–5]. However, ZnO has a large band gap, which not only limits its use of visible light, but also makes it easier for electrons to combine with holes, thus reducing the performance of the material. It is found that doping a proper amount of metal or nonmetal elements into ZnO semiconductor materials can significantly improve their properties [6–8]. The transition element doped zinc oxide can increase the defect density and improve the photoelectric performance of zinc oxide. Copper is the most widely studied because it is adjacent to zinc in the periodic table [2,9,10]. The radius of nickel ions is close to that of zinc ions, and the price of electricity is the same as that of zinc. It is found that nickel ions will replace zinc ions, which will cause distortion of the crystal lattice of zinc oxide and affect the microscopic morphology of zinc oxide, and it will cause red shift of UV luminescence peak [11].

In the method of synthesizing zinc oxide, due to the low temperature, simple operation, low cost, and good crystallinity of the hydrothermal synthesis method, transition elements doped ZnO nanomaterials has become a research focus of scholars in recent years [12]. Available research on nickel doped zinc oxide is quite limited, focusing mostly on magnetic properties [13,14], Unfortunately, up to now, the mechanism of the effect on electrochemical and optical properties caused by Ni atom and the roles of Ni in ZnO are

* Corresponding author.
E-mail addresses: lyrenfz@163.com (F. Ren), volinsky@usf.edu (A.A. Volinsky).

https://doi.org/10.1016/j.ijleo.2020.165204
Received 18 April 2020; Accepted 7 July 2020

still not reported.

Transport and optical properties of semiconductors are greatly dominated by the electronic states in the neighborhood of the band gap [15,16]. In order to explain, predict and optimize the properties

of Ni-doped ZnO systems, it is necessary to understand the nature of the electronic properties of Ni-doped ZnO. This paper is aimed at this problem. The Ni-doped ZnO is prepared by hydrothermal method. The effect of nickel on the optical and electrochemical properties of zinc oxide is systematically studied. The combination of theoretical and experimental results provides important information for future doping research and applications reference.

2. Experimental details and model construction

2.1. Experimental details

In this experiment, Ni-doped zinc oxide was prepared by hydrothermal method. Firstly, FTO substrate was cleaned and mixed solution of zinc acetate and hexamethylenetetramine with a concentration of 0.05 mol/L was prepared. FTO substrate was put into the mixed solution and stirred at low speed at room temperature using a magnetic stirrer. Forming a seed crystal layer. The treated FTO substrate was then annealed at 350℃ for 1 h. 20 mL of a mixed solution of zinc acetate and hexamethylenetetramine with equal molar concentration is prepared, the annealed FTO substrate is obliquely placed in the inner lining of the reaction kettle, and is taken out after hydrothermal reaction at 95 DEG C for 6 h. The preparation of nickel-doped zinc oxide requires adding nickel nitrate solution with corresponding concentration into the mixed solution. Three groups of samples were prepared by adjusting nickel nitrate D8 Advance X- ray diffractometer (XRD) was used to detect the phase composition of the sample. Cu target k, tube voltage 40 kV, tube current 40 mA, $\lambda = 0.15418$ nm, step size 0.02, and 2 θ angle range 20–75.JSM-5610LV scanning electron microscope (SEM, 20 kV) was used to observe the microstructure morphology of the sample, and the accompanying energy dispersive spectrometer (EDS) was used to detect the element types contained in the micro-area sample. JEOL JEM-2010 F transmission electron microscope (TEM, 200 kV) was used to detect the particle size and microcrystalline structure of the sample. The photoluminescence (PL) properties of the samples were tested by F-280 fluorescence spectrophotometer. Electrochemical performance was tested by electrochemical workstation (CHI660D, Beijing Join Technology Co., Ltd).

2.2. Model construction

The model constructed in this paper is a pure ZnO ($1 \times 1 \times 1$) unit cell model, the corresponding doping amount is 0, the ($3 \times 3 \times 2$) corresponding doping amount of one Ni atom replacing Zn atom is 0.0278 and ($2 \times 2 \times 3$) corresponding doping amount of one Ni atom replacing Zn atom (the corresponding doping amount is 0.0417); The crystal structure is shown in Fig. 1:

The calculations are based on the ultrasoft and norm-conserving pseudopotentials available in the CASTEP code to optimize the models and obtain the authentic optical properties [17,18]. When describing the interaction between ion real and valence electrons, the selected valence electron configuration are O: 2 $s^2 2p^4$, Zn: $3d^{10}4s^2$, Ni: $3d^8 4s^2$, and other electrons are considered as core electrons for calculation. In this paper, GGA + U method is used to correct the band gap [19–22]. The selected parameters are Zn's d orbit plus 5 eV (U^{Ti} d = 5 eV), O's P orbit plus 8 eV (U^{O} p = 8 eV). In the calculation, the crystal structure is optimized first, and the electronic structure and optical properties are calculated according to the obtained structural parameters.

3. Results and discussions

3.1. XRD and SEM of samples

Fig. 2 is the XRD diffraction patterns of nickel-doped zinc oxide film. All three film have diffraction reflections corresponding to (100), (002) and (101) planes, and there are no impurities, indicating that the film prepared by the experiment is pure zinc oxide, and all doped samples maintain the wurtzite structure of ZnO. As the Ni doping concentration increases, the intensity of the (100) and

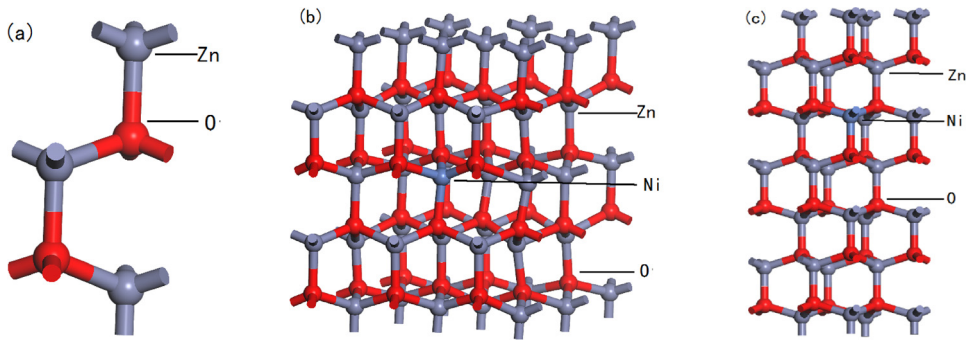

Fig. 1. The models of: a) pure ZnO b)$Ni_{0.0278}Zn_{0.99722}O$ c) $Ni_{0.0417}Zn_{0.9583}O$.

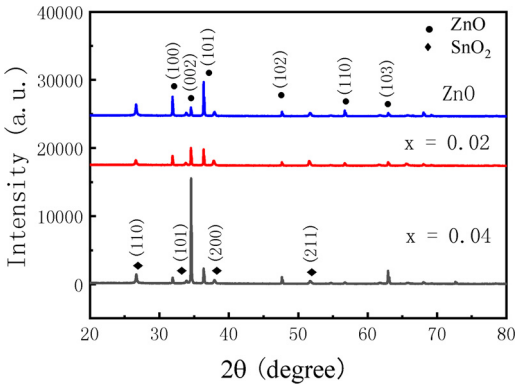

Fig. 2. XRD spectrum of $Ni_XZn_{1-X}O$.

(101) planes gradually increased, and the intensity of the (002) planes decreased. Ni affects the C-axis orientation of the zinc oxide film. The higher the Ni ion concentration, the more obvious the effect. The angle of the diffraction peaks was shifted slightly after the addition of Ni, indicating that nickel may enter the zinc oxide lattice structure and cause structural distortion. Fig. 3 is a SEM image of the sample, it can be seen that the ends of the zinc oxide film prepared by the hydrothermal method show regular hexagons. As the nickel doping concentration increases, the hexagonal size increases. This shows that nickel can promote the lateral growth of zinc oxide rods.

3.2. Photoluminescence (PL) analysis

Fig. 4 is a photoluminescence spectrum of a Ni-doped zinc oxide film. It can be seen that the film has three fluorescence emission bands, namely, a purple band with a center wavelength of about 400 nm, a blue-purple band with a center wavelength of about 455 nm, and a blue band with a center wavelength of about 470 nm.As can be seen from the figure, with the doping of nickel, the overall luminous intensity shows a trend of decreasing first and then increasing, but on the whole, the emission peak decreases obviously after doping nickel, which may be due to the modification of the energy level of zinc oxide by the introduction of nickel, or due to the introduction of nickel into its own energy level [23]. Compared with the three curves, there is no excess emission peak after nickel doping. It is possible that nickel ions and zinc ions are bivalent, and their radii are similar, resulting in less lattice distortion, while other defects are not derived after substitution doping.

3.3. UV–vis Spectrum analysis

Fig. 5 are transmission and absorption spectra with $Ni_XZn_{1-X}O$ films. It can be seen from the Fig. 5(a) that the light transmission intensity of zinc oxide is the lowest in the range of less than 380 nm. when the wavelength is greater than 380 nm, the corresponding light absorption intensity of the three groups of samples is $Ni_{0.04}Zn_{0.96}O > ZnO > Ni_{0.02}Zn_{0.98}O$ in the visible range, and the transmittance of the $Ni_{0.02}Zn_{0.98}O$ film is the highest in the whole wavelength range. It can be seen from the Fig. 5(b) that the absorption rate of the zinc oxide film is relatively large in the range of 280 − 380 nm, while the absorption rate starts to decrease in the range of 380 nm or more. This is the opposite of the transmittance result. The band gap of the material can be calculated according to Formula (1) [24,25]. The calculation results are shown in Table 1. it can be seen that the band gap of pure zinc oxide film is 3.26 eV. With the increase of Ni^{2+} doping concentration, the band gap tends to decrease first and then increase. This change trend is consistent with the later calculation results.

$$Ahv = c(hv\text{-}Eg)^{1/2} \quad (1)$$

Where α is the absorption coefficient, hv is the photon energy, c is the speed of light and Eg is the band gap.

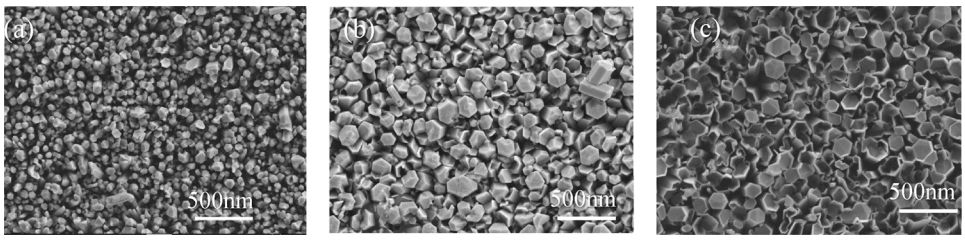

Fig. 3. SEM of $Ni_XZn_{1-X}O$. (a) x = 0 (b) x = 2 (c) x = 4.

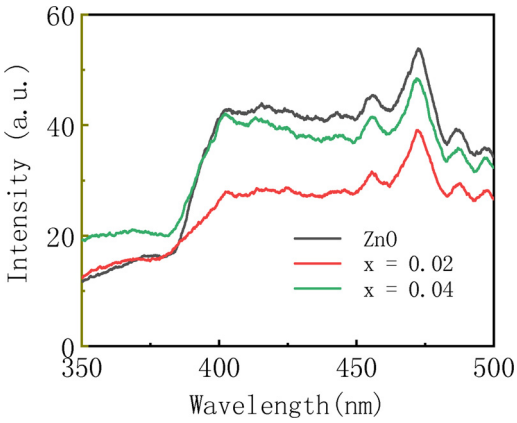

Fig. 4. PL spectra of $Ni_XZn_{1-X}O$ films.

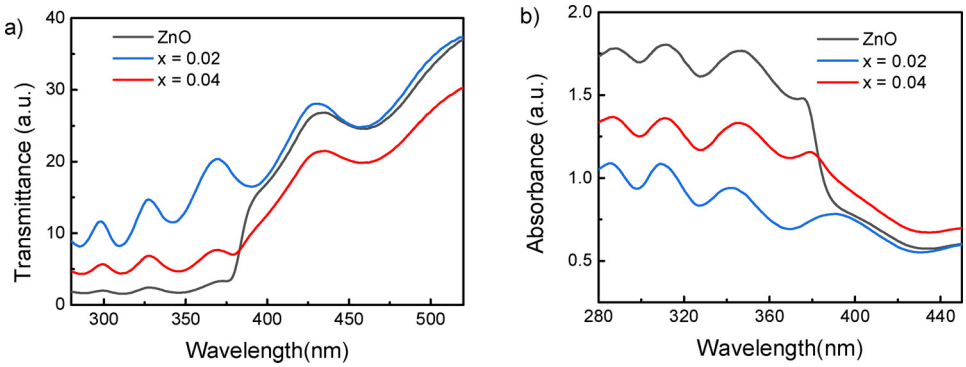

Fig. 5. a) Transmission spectrum b) absorption spectrum.

Table 1
band gap of $Ni_XZn_{1-X}O$ films.

x	0	2	4
Band gap /eV	3.26	2.64	2.75

3.4. Electrochemical analysis

Fig. 6 is an M–S(Mott-Schottky) plots, which is tangent to the longest straight line portion of the curve, and the slope is positive, indicating that the Ni-doped zinc oxide prepared in this paper is an n-type semiconductor. The donor density of semiconductor can be

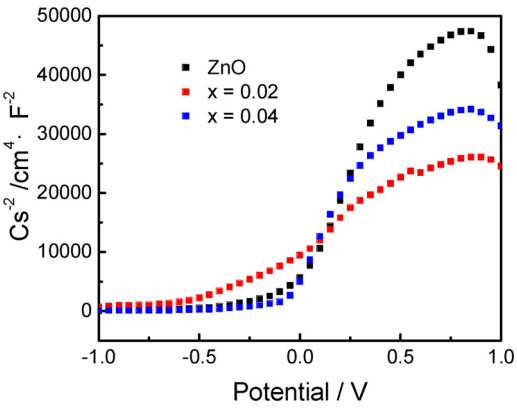

Fig. 6. M-S Plots of $Ni_XZn_{1-X}O$ films.

Table 2
Flat -band Potential and Conducted band Potential.

Ni^{2+} concentration /%	0	2	4
Flat charged potential /eV	−0.1	−0.5	−0.15
conduction band potential /eV	0−0.2	−0.4 – -0.2	−0.05–0.15
Valence band potential /eV	3.26–3.46	2.24–2.44	2.70–2.90

calculated by formula (2) [26,27]. From Eq. (2), it can be concluded that the donor density is the slope of the tangent. The larger the slope is, the higher the donor density is. In the three curves, when the content of Ni is low, the donor density is sharply increase, and when the content of Ni is further increased, the donor density is decreased. The higher N_D means more charge separation, less charge recombination, increased charge collection rate and longer electron lifetime. Therefore, the doping of a small amount of nickel is beneficial to improve the performance of zinc oxide.

The flat band potential E_{FB} can be found by the intercept on the abscissa. For the n-type semi-conductor, the flat - band potential is 0.1 − 0.3 eV positive than the conduction band potential, and the potential of the flat band potentiometer obtained from the MS curve is shown in Table 2. It can be concluded from Fig. 5 and Table 2. It can be concluded that the pure ZnO is −0.1 eV, and the horizontal potential decreases to different degrees after Ni doping.

$$\frac{1}{C_{sC}^2} = \frac{2}{eN\varepsilon_0\varepsilon_r}\left(E - E_{FB} - \frac{KT}{e}\right) \tag{2}$$

Where C_{SC} is capacitance of the space charge region, ε_r is dielectric constant of the semiconductor, ε_0 is permittivity of free space (885 $\times$ 10^{-14} F/m), which is the dielectric constant of semiconductor at room temperature. In this paper, 15.6 is taken, N is donor density (electron donor concentration for an n-type semiconductor or hole acceptor concentration for a p-type semiconductor), E_{FB} is flat-band potential, E is applied potential, K is the Boltzmann constant (K = 1.38 $\times$ 10^{-23} J/K), T is temperature, e is electronic charge (1.602 $\times$ 10^{-19} C), and KT/e is about 25 mv at room temperature, which can be ignored.

3.5. Energy band structure and electron density of states analysis

Fig. 7 is the band structure of Ni-doped zinc oxide calculated by the first principle. It can be seen that the band gap of pure zinc oxide is 3.372 eV, which is very close to the theoretical value. With the doping of Ni, the band gap decreases first and then increase, which is consistent with the above experiment results. The density of states (Fig. 8) shows that in pure zinc oxide, Zn-4 s orbital electrons interact with O-2p orbital electrons to form s-like inverse bonds and p-like bonds, forming band gap. After Ni doped, the Fermi level enters the conduction band in different degrees, which is consistent with the calculation results in Table 2. The 2 s distribution of oxygen atoms is around -15 eV, with a width of 1 eV. The band is narrow, showing strong localization and no obvious interaction with energy levels in other valence bands. The conduction band is mainly due to the 3d contribution of Ni atoms, and impurity energy levels are formed, so the conduction band moves down, which reduces the band gap to different degrees compared with pure zinc oxide. Several independent energy levels appeared at the valence band close to Fermi level. Compared with the density of states diagram, it can be seen that the contribution is mainly from the 3d state of Ni. The energy level can act as a springboard for electrons to transition from valence band to impurity level and then to conduction band, reducing the energy required in the electron transition process. When x = 0.0417, the band gap slightly increases. Comparing the density of states results, it can be seen that the impurity level formed near the Fermi level slightly moves up the valence band due to the large doping amount, and this result is also consistent with the calculation results in Table 2.

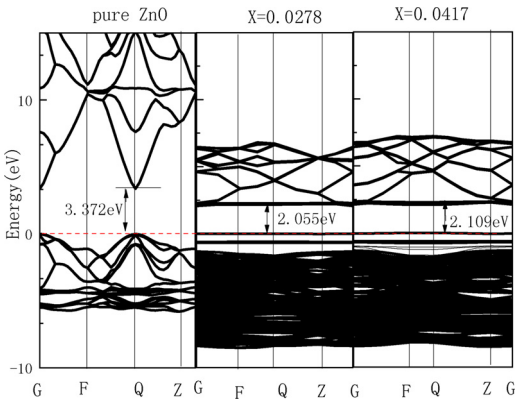

Fig. 7. Band structure of $Ni_XZn_{1-X}O$.

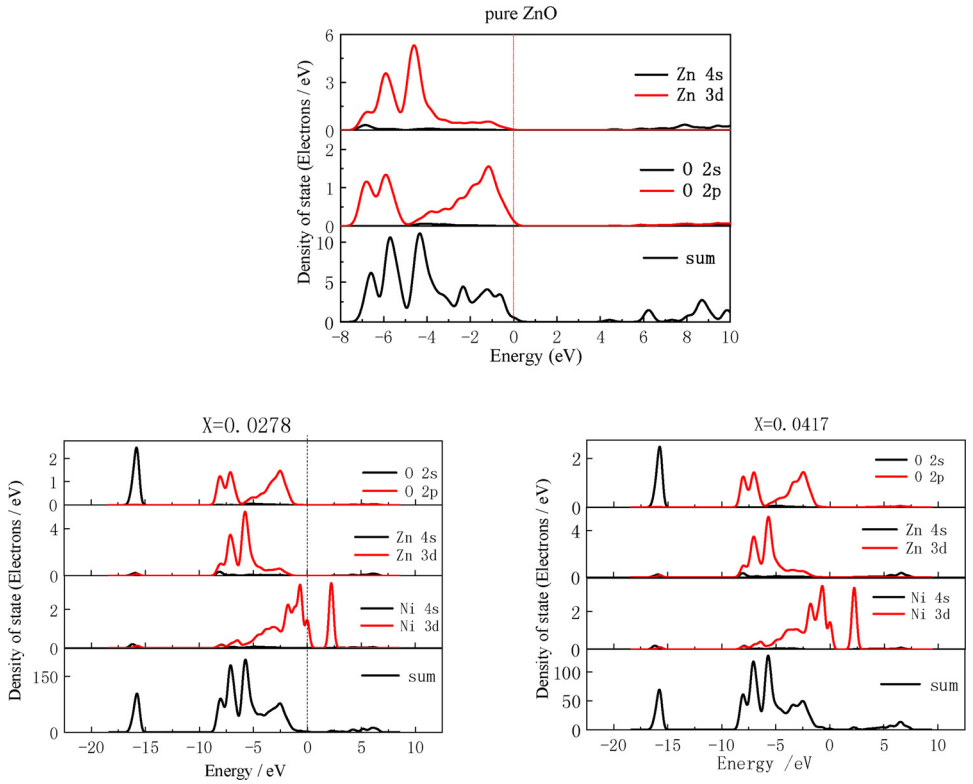

Fig. 8. PDOS of $Ni_XZn_{1-X}O$.

4. Conclusion

In this paper, Ni-doped ZnO thin films were prepared by hydrothermal method. After experiment and theoretical calculation, with the doping of Ni, the luminous decreases first and then increase, and the emission peaks decrease significantly after nickel doping. The band gap of the sample obtained from the light absorption spectrum decreases first and then decreases with the increase of Ni^{2+} doping concentration. According to the M–S (Mott - Schottky) curve, the Ni-doped zinc oxide prepared in this paper is an n-type semiconductor. When the content of Ni is low, the donor density will increase sharply due to nickel doping. When the content of Ni increases again, the donor density will decrease instead. From the calculated results of energy band and density of states, it can be seen that with the increase of nickel doping amount, the band gap decreases first and then increase. The reason for the decrease is that the impurity level formed by nickel doping moves the conduction band down, and then the band gap increases because the impurity level slightly moves the valence band up.

Author contributions

Zhanhong Ma drafted the manuscript and performed the experiments; Fengzhang Ren and Yafeng Deng contributed to the conception of the study; Alex A. Volinsky performed the data analysis and revised the manuscript.

Funding

This study was supported by the Henan International Science and Technology Cooperation Program (152102410035), the Program for Science and Technology Innovation Talents in Universities of the Henan Province (17HASTIT026), Education Department of the Henan Province (16A430005) and the Program for Changjiang Scholars and Innovative Research Team in University (IRT_16R21).

Declaration of Competing Interest

None.

References

[1] H.X. Peng, G.X. Liu, X.T. Dong, W. Yu, Preparation and characteristics of Fe_3O_4@YVO_4: Eu^{3+} Bi functional magnetic-luminescent nanocomposites, J. Alloys Compd. 509 (2011) 6930–6934, https://doi.org/10.1016/j.jallcom.2011.04.004.

[2] X.L. Li, X.H. Xu, Z.Y. Quan, J.F. Guo, H.S. Wu, G.A. Gehring, Role of donor defects in enhancing ferromagnetism of Cu-doped ZnO films, J. Appl. Phys. 105 (2009) 103914–103919, https://doi.org/10.1063/1.3130104.

[3] H.L. Liu, X. Cheng, H.B. Liu, J.H. Yang, Y. Liu, X.Y. liu, G. Ming, M.B. Wei, X. Zhang, Y.H. Jiang, Structural, optical and magnetic properties of Cu and V co-doped ZnO nanoparticles, Physica E. 47 (2013) 1–5, https://doi.org/10.1016/j.physe.2012.09.019.

[4] H.F. Acosta, R.C. Pitalúa, O. Almanza, Electron paramagnetic resonance in $Zn_{1-x}Co_xO$, J. Magn. Magn. Mater. 329 (2013) 39–42, https://doi.org/10.1016/j.jmmm.2012.10.026.

[5] Z.H. Ma, F.Z. Ren, Y.F. Deng, A.A. Volinsky, Experimental and theoretical studies of $K_xZn_{1-x}O$, Ceram. Int. 46 (2020) 763–767, https://doi.org/10.1016/j.ceramint.2019.09.030.

[6] F.Y. Ran, M. Tanemura, Y. Hayashi, Effect of substrate temperature on the room-temperature ferromagnetism of Cu-doped ZnO films, J. Cryst. Growth 31 (2009) 4270–4274, https://doi.org/10.1016/j.jcrysgro.2009.07.008.

[7] T.Y. Tang, J.Q. Zhang, Study on band structure and spectrum of $Mg_xZn_{1-x}O$ based on first principles, J. Nanoelectron. Optoelectron. 13 (2018) 646–652, https://doi.org/10.1166/jno.2018 2333.

[8] J.H. Zheng, J.L. Song, Q. Jiang, J.S. Lian, Optical properties of Cu-doped ZnO nanoparticles experim- ental and first-principles theory research, J Mater Sci.-Mater Electron. 23 (2012) 1521–1524, https://doi.org/10.1007/s10854-012-0622-z.

[9] Z.H. Ma, F.Z. Ren, X.L. Ming, Y.Q. Long, A.A. Volinsky, Cu-Doped ZnO electronic structure and optical properties studied by first-principles calculations and experiments, Materials 12 (2019) 196, https://doi.org/10.3390/ma12010196.

[10] S. Muhammad, I. Ulah, M.I. Khan, J. Khan, M.T. Qureshi, Structural and optical properties of pure and copper doped zinc oxide nanoparticles, Results Phys. 9 (2018) 1301–1309, https://doi.org/10.1016/j.rinp.2018.04.010.

[11] Xl. Xu, X.T. He, X.Y. Fu, X.H. He, Hydrothermai synthesis and performance characterization of Ni^{2+} doped ZnO array films, J. Syn. Crys. 43 (2014) 502–507 in Chinese.

[12] M. Sudha, S. Radha, S. Kirubaveni, N. Santhosh, Experimental study on structural, optoelectronic and room temperature sensing performance of nickel doped ZnO based ethanol sensors, Solid State Sci. 78 (2018) 30–39, https://doi.org/10.1016/j.solidstatesciences.2018 02.004.

[13] K. Jeyasubramaniana, R.V. Williamb, P. Thiruramanathanc, G.S. Hikku, M. Kumar Vimal, B. Ashima, Dielectric and magnetic properties of nanoporous nickel doped zinc oxide for spintronic applications, J. Magn. Magn.Mater. 485 (2019) 27–35, https://doi.org/10.1016/j.jmmm.2019.04.032.

[14] P.R. Chithira, T.T. John, Defect and dopant induced room temperature ferro-magnetism in Ni doped ZnO nanoparticles, J. Alloys Compd. 766 (2018) 572–583, https://doi.org/10.1016/j.jallcom.2018.06.336.

[15] K. Hoang, S.D. Mahanti, M.G. Kanatzidis, Impurity clustering and impurityinduced bands in PbTe-, SnTe-, and GeTe - based bulk thermoelectric, Phys. Rev. B 81 (2010) 115106–115120, https://doi.org/10.1103/PhysRevB.81.115106.

[16] Y. Kim, S. Kang, Effect of particle size on photoluminescence emission intensity in ZnO, Acta Mater. 59 (2011) 3024–3031, https://doi.org/10.1016/j.actamat.2011.01.042.

[17] W. Kohn, L.J. Sham, Self-consistent equations including exchange and correlation effects, Phys. Rev. 140 (1965) 1133–1138, https://doi.org/10.1103/PhysRev.140.A1133.

[18] M.C. Payne, M.P. Teter, D.C. Allan, Iterative minimization techniques for ab initio total-energy calculations molecular dynamics and conjugate gradients, Rev. Mod. Phys. 64 (1992) 1045–1094, https://doi.org/10.1103/RevModPhys.64.1045.

[19] S.Q. Guo, Q.Y. Hou, C.W. Zhao, F. Mao, First principles study of the effect of high V doping on the optical band gap and absorption spectrum of ZnO, Acta Phys. Sin. 63 (2014) 107101, , https://doi.org/10.7498/aps.63.107101.

[20] Q. Hou, D.M. Xi, W.L. Li, X.F. Jia, Z.C. Xu, First-principles research on the optical and electrical properties and mechanisms of In-doped ZnO, Phys. B Condens. Matter. 537 (2018) 258–266, https://doi.org/10.1016/j.physb.2018.02.026.

[21] Y. Li, Q. Hou, C.W. Zhao, Z.C. Xu, Study on electrical structure and magneto-optical properties of W-doped ZnO, J. Magn.Magn. Mater. 451 (2018) 697–703, https://doi.org/10.1016/j.jmmm.2017.12.012.

[22] J. Wen, J. Zhang, Z. Qiu, X. Yang, Z.Q. Li, The investigation of Ce doped ZnO crystal: the electronic, optical and magnetic properties, Phys B Condens Matter. 534 (2018) 44–50, https://doi.org/10.1016/j.physb.2018.01.035.

[23] A. Gupta, N.K. Verma, H.S. Bhatti, Fast photoluminescence decay processes of doped ZnO phosphors, Appl. Phys. B 87 (2007) 311–315, https://doi.org/10.1007/s00340-007-2582-1.

[24] Y.F. Deng, Z.H. Ma, F.Z. Ren, G.X. Wang, A.A. Volinsky, Enhanced morphology and photoelectric properties of one-dimensional TiO_2 nanorod array films, Chem. Phys. Lett. 724 (2019) 42–49, https://doi.org/10.1016/j.cplett.2019.03.054.

[25] J.N. Ben, R. Ouertani, W. Chakhari, R. Chtourou, Photo-electrochemical properties of Sb_2S_3/TiO_2 heterostructures integrally synthesis by hydrothermal method, J. Mate.- Sci.Mater. Electron. 30 (2019) 5631–5639, https://doi.org/10.1007/s10854-019-00856-6.

[26] Y.F. Deng, Z.H. Ma, F.Z. Ren, G. X.Wang, Enhanced photoelectron-chemical performance of TiO_2 nanorod array films based on TiO_2 compact layers synthesized by a two-step method, RSC Adv. 9 (2019) 21777–21785, https://doi.org/10.1039/c9ra03755a.

[27] Y.F. Deng, Z.H. Ma, F.Z. Ren, G.X. Wang, Improved photoelectric performance of DSSCs based on TiO_2 nanorod array/Ni-doped TiO_2 compact layer composites film, J. Solid State Electrochem. 23 (2019) 3031–3041, https://doi.org/10.1007/s10008-019-04399-y.